

COMPARISON OF FRACTIONAL AND GEODESIC ANISOTROPY IN DIFFUSION TENSOR IMAGES OF 90 MONOZYGOTIC AND DIZYGOTIC TWINS

Agatha D. Lee¹, Natasha Lepore¹, Marina Barysheva¹, Yi-Yu Chou¹, Caroline Brun¹, Sarah K. Madsen¹, Katie L. McMahon², Greig I. de Zubicaray², Matthew Meredith², Margaret J. Wright³, Arthur W. Toga¹, Paul M. Thompson¹

¹Laboratory of Neuro Imaging, Department of Neurology, UCLA School of Medicine, Los Angeles, CA

²Functional MRI Laboratory, Centre for Magnetic Resonance, University of Queensland, Brisbane, Australia

³Queensland Institute of Medical Research, Brisbane, Australia

ABSTRACT

We used diffusion tensor magnetic resonance imaging (DTI) to reveal the extent of genetic effects on brain fiber microstructure, based on tensor-derived measures, in 22 pairs of monozygotic (MZ) twins and 23 pairs of dizygotic (DZ) twins (90 scans). After Log-Euclidean denoising to remove rank-deficient tensors, DTI volumes were fluidly registered by high-dimensional mapping of co-registered MP-RAGE scans to a geometrically-centered mean neuroanatomical template. After tensor re-orientation using the strain of the 3D fluid transformation, we computed two widely used scalar measures of fiber integrity: fractional anisotropy (FA), and geodesic anisotropy (GA), which measures the geodesic distance between tensors in the symmetric positive-definite tensor manifold. Spatial maps of intraclass correlations (r) between MZ and DZ twins were compared to compute maps of Falconer's heritability statistics, i.e. the proportion of population variance explainable by genetic differences among individuals. Cumulative distribution plots (CDF) of effect sizes showed that the manifold measure, GA, comparably the Euclidean measure, FA, in detecting genetic correlations. While maps were relatively noisy, the CDFs showed promise for detecting genetic influences on brain fiber integrity as the current sample expands.

Key Words— Fractional Anisotropy, Geodesic Anisotropy, Twin

1. INTRODUCTION

Diffusion tensor (DT) MR images can measure water diffusion in tissue, providing vital information on fiber connectivity and composition in the healthy and diseased brain. Simple scalar measures, derived from the diffusion tensor, such as the trace or mean diffusivity, can adequately describe isotropic water diffusion, which only occurs in brain regions such as the cerebrospinal fluid. In the white matter, myelinated fibers resist diffusion orthogonal to the local dominant fiber orientation, thus diffusion occurs preferentially along local fiber tracts. In clinical research, white matter fiber integrity is commonly assessed by determining how strongly diffusion is directionally constrained. Of the directional diffusion measures, fractional anisotropy (FA), computed from the DT eigenvalues, is widely used in neuroscientific studies. FA is generally reduced in diseases that affect fiber integrity (e.g., Alzheimer's disease), and may be used to map disease effects on white matter. A related scalar measure, Geodesic Anisotropy (GA) [3], has recently been developed as an

alternative to FA. GA measures the distance of a diffusion tensor to the nearest isotropic tensor, and is computed intrinsically on the manifold of positive-definite symmetric diffusion tensors. Here we used maps of FA versus GA to characterize microstructural differences and similarities in a DTI database of 90 healthy young adult twins.

While variations in DTI signals across subjects are the topic of intensive investigation, there is a need to discover which fiber characteristics are genetically influenced, and ultimately which genes influence fiber integrity. A first step in this quest is to determine (1) which DTI measures are genetically influenced; and (2) what is the relative proportion of genetic versus environmental control over fiber characteristics in different brain regions. Both of these questions can be answered, in principle, using DTI scans of twins. A practical benefit of knowing where DTI signals are genetically controlled is to determine the added power of a discordance design to isolate disease-specific features, in which patients are compared with healthy family members, rather than with unrelated control subjects. To our knowledge, only one study [9] has examined genetic influences on DTI, and found that the proportion of genetic and environmental control varied regionally, for the fractional anisotropy of the corpus callosum. Here we extended this approach to create initial steps toward 3D maps of genetic influences on DTI signals, evaluating which measure, FA or GA, gives greater effect size for detecting genetic influences. The answer to this question depends on (1) empirical factors such as the noise in each channel of the matrix-valued signals, and (2) mathematical factors such as the correct combination of the tensor components using statistics on associated Lie groups including the symmetric tensor manifold. Both FA and GA have been proposed as fiber integrity measures in clinical studies, so it is valuable to know the extent to which genetic factors determine the normal population variability in these measures.

Twin studies using conventional MRI [9,10] have found that several aspects of brain morphometry are under strong genetic control, including cortical thickness and regional gray and white matter volumes. To our knowledge, no 3D maps have been published that visualize genetic influences on diffusion profiles or fiber anisotropy using DTI.

Here we use DTI-derived maps of FA and GA to compute maps of the intraclass correlation (r) of MZ and DZ twins at each voxel. This enables us to assess genetic effects on white matter microstructure, from the correlations in different types of twins, visualizing the profile of genetic influences in 3D.

2. METHODS

2.1. Subject description and image acquisition

3D structural brain MRI scans and DT-MRI scans were acquired from 90 subjects: 22 pairs of monozygotic twins (MZ; 20 males/24 females; 25.1±1.5SD years old) and 23 pairs of dizygotic twins (DZ; all same-sex pairs; 20 males/26 females; 23.5±2.2 years) on a 4T Bruker Medspec MRI scanner with an optimized diffusion tensor sequence [4]. Imaging parameters were: 21 axial slices (5 mm thick), FOV = 23 cm, TR/TE 6090/91.7 ms, 0.5 mm gap, with a 128×100 acquisition matrix. 30 directional gradients were applied: three scans with no diffusion sensitization (i.e., T2-weighted images) and 27 diffusion-weighted images for which gradient directions were evenly distributed on the hemisphere [7]. The reconstruction matrix was 128×128, yielding a 1.8×1.8 mm² in-plane resolution. Total scan time was 3.05 minutes.

2.2. Image Preprocessing and Registration

3D structural MR images were automatically skull-stripped using the Brain Surface Extraction software (BSE) [10] followed by manual editing. The masked image was registered via 9-parameter linear transformation to a high resolution single-subject brain template image, the Colin27 template, using the FLIRT software [6]. A Minimal Deformation Target (MDT) image was generated from the 90 subjects using nonlinear registration, and each 3D structural image was warped to the MDT using a 3D fluid registration that allows large-deformation diffeomorphic mappings [4,8]. Jacobian matrices were obtained from the resulting deformation fields.

Diffusion Tensors (3×3 positive symmetric matrices) were computed from DICOM DT-MR images and smoothed using Log-Euclidean tensor denoising to eliminate singular, negative definite, or rank-deficient tensors, using MedINRIA (<http://www.sop.inria.fr/asclepios/software/MedINRIA>). To eliminate extracerebral tissues, a diagonal component image (D_{xx}) was manually stripped of nonbrain tissues, yielding a binary brain extraction mask (cerebellum included). Masked images were registered by 9-parameter transformation to the corresponding 3D structural images in the standard template space using FLIRT software [6].

2.3. Handling orientation information

Transformation parameters from affine and nonlinear registrations were used to rotationally reorient the tensors at each voxel [1] to ensure that the multidimensional tensor orientations remained consistent with the anatomy after image transformation [1,11]. Two separate methods were used to compute the tensor rotations. First, the finite Strain (FS) method was applied using the transformation matrix M resulting from the affine registration. A preservation of principal direction (PPD) algorithm was then applied to the higher-order transformation, as in [1] and [12].

More precisely, to find the rotational component R_r , of the affine transformation, we used

$$R_r = \operatorname{argmin}_{Q'} \|Q' - M\| = \frac{M}{\sqrt{MM^T}} \quad (1)$$

Reorientation components for the nonlinear transformation (R_n) were computed using the Jacobian matrix (J) from the fluid

registration step for the MP-RAGE MR images. The principal orientation of the primary (e_1) and secondary (e_2) eigenvectors were computed from the DT images, as in [2]:

$$R_n = R_{n1} \cdot R_{n2}, \quad (2)$$

$$R_{n1}e_1 = \frac{Je_1}{\|Je_1\|},$$

$$R_{n2}e_2 = \frac{Je_2 - (Je_2 \cdot Je_1)Je_1}{\|Je_2 - (Je_2 \cdot Je_1)Je_1\|}.$$

2.4. Scalar statistics in the Log-Euclidean space.

Positive definite Diffusion Tensors do not form a vector space under the usual operations of matrix addition and scalar multiplication. **Figure 1** illustrates the ‘Log-Euclidean framework’ [2], which has been proposed to simplify computations for positive definite tensor statistics. In this framework, the tensor manifold is projected to its tangent plane at the origin, where standard vector space statistics can be used [2, 8]. A typical measure of diffusion anisotropy is the fractional anisotropy (FA),

$$FA = \frac{\sqrt{3}}{\sqrt{2}} \frac{\sqrt{(\lambda_1 - \langle \lambda \rangle)^2 + (\lambda_2 - \langle \lambda \rangle)^2 + (\lambda_3 - \langle \lambda \rangle)^2}}{\sqrt{\lambda_1^2 + \lambda_2^2 + \lambda_3^2}} \quad (3)$$

with

$$\langle \lambda \rangle = \frac{\lambda_1 + \lambda_2 + \lambda_3}{3}. \quad \text{FA, however, is an extrinsic measure on}$$

the manifold of symmetric positive definite tensors. Geodesic anisotropy (GA) is derived from the tensor manifold metric [3]. Here, we used GA computed in the Log-Euclidean metric [8] as an alternative scalar measure to compare with FA. GA, in our work, is defined as:

$$GA(S) = \sqrt{\operatorname{Trace}(\log S - \langle \log S \rangle)^2}, \quad (4)$$

$$\text{With } \langle \log S \rangle = \frac{\operatorname{Trace}(\log S)}{3}.$$

FA is based on a simple comparison of the tensor eigenvalues. GA, however, measures the deviation of the tensor from the ‘nearest’ isotropic tensor in the associated Log-Euclidean metric. GA may be seen as the geodesic distance on the tangent plane at the origin of the tensor manifold. **Figure 1** illustrates the difference between the geodesic (intrinsic) distance (*green solid line on the manifold*) and the Euclidean (extrinsic) distance (*olive colored dotted line*). We renormalized GA by applying the hyperbolic tangent transformation to the GA values (tGA) as in [3], to create maps with a comparable range to the FA.

2.5. Statistical analysis of structural models for twins

Voxelwise FA and GA values were computed for all 90 fluidly registered tensor images. The intraclass correlation (r) can be used to quantify similarity in paired data, such as the twin data here. Intraclass correlations for the MZ group (r_{MZ}) and for the DZ group (r_{DZ}) were computed at each voxel for both FA and GA. To compute the proportion of the variance in the FA (and GA) values attributable to genetic differences among individuals, we used a measure known as Falconer’s heritability estimate [5]:

$$h^2 = 2(r_{MZ} - r_{DZ}) \quad (5)$$

This parameter, which is expected to vary across brain regions and for different DTI measures, allows inferences to be made about how much of the population variance is attributable to genetic factors, as opposed to that due to environmental factors (e.g., nutrition, *in utero* environment) and measurement errors or inter-subject registration errors.

3. RESULTS

Figure 2 shows mean maps of FA and tGA maps for *all* 44 MZ subjects and for all 46 DZ subjects. The ratio of the DZ to MZ group means (DZ/MZ) for each scalar measure was close to 1. As is necessary in twin studies, the mean values for these parameters were very similar within groups of different zygositys.

To examine the intra-pair variance within each of the groups, **Figures 3a** and **3c** show intraclass correlation (r) maps between MZ pairs and DZ pairs computed from tGA. **Figure 3b** and **3d** display maps of correlations between MZ pairs and DZ pairs computed from FA. Although the ventricles, corpus callosum and some anterior temporal regions show higher resemblance among MZs compared to DZ in maps from both FAs and tGAs, all maps are extremely noisy. Falconer's heritability estimate, computed at each voxel, is also shown in **Figure 3**. Heritability maps for both tGA and FA show that the fiber characteristics in the corpus callosum and some anterior temporal regions may be heritable, as shown in **Figure 3e** and **3f**. This is not unreasonable, as these are also heavily myelinated white matter tracts with highest FA (and GA). Heritable regions are slightly more extensive for tGA (**3e**) than FA (**3f**), but both maps are very noisy.

Figures 4a-d show significance value maps for these correlations, based on the computed r values; significance was assigned using a non-parametric permutation test at each voxel for both FA and GA. Correlation is the strongest in the corpus callosum and some of anterior temporal regions.

Cumulative distribution functions (CDFs; **Fig. 5**) show p -values for the FA and tGA statistics in each twin group. The solid black line, for comparison, indicates the null distribution, which would represent a complete lack of correlation between twins. The difference between the null distribution and the empirical CDF curve reflects the distribution of voxels with different significance levels, which may be considered as a measure of the effect size in maps thresholded at different levels. Statistics from the GA yielded significance CDFs with similar slopes at the origin than those for FA, which is a simpler, Euclidean, anisotropy measure. Although we expected that the GA might help detect genetic effects with higher power than the FA, as the effect size in the MZ correlation map were comparable.

5. DISCUSSION

Here we introduced an algorithmic pipeline to map genetic influences on fiber diffusion anisotropy in twins, using 3D fluid registration, Log-Euclidean mappings, and voxel-based quantitative genetics. The rather low signal-to-noise in the statistical maps, even with $N=90$ subjects, likely results from (1) the small variance in FA and GA in healthy young subjects, (2) possibly higher environmental (nongenetic) influences; and (3)

registration errors across subjects, which is inevitable as no perfect homology exists between fiber paths across subjects. In 90 twins, GA slightly outperformed FA showed comparable results for detecting twin correlations, although effect sizes were rather weak (correlations occurring at around 4-6 times the chance level for GA in MZ twins, which would not satisfy false discovery rate criteria for overall significance). This sample will expand ten-fold to 1150 subjects over 5 years, suggesting that power may be sufficient to improve the CDFs (**Fig. 5**) and create heritability maps for fiber parameters.

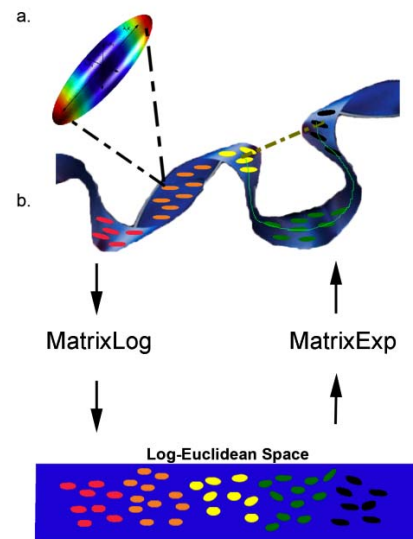


Figure 1(a) shows the diffusion tensor at one voxel, represented using an ellipsoidal shape; colors denote distances of boundary points to the origin, indicating relative rates of diffusion in each direction. The ellipsoid's axes indicate the 3 orthogonal eigenvectors, whose length is given by the corresponding eigenvalues. Positive definite symmetric tensors [ellipses in **(b)**] lie in a non-linear manifold in \mathbb{R}^6 . Because symmetric, positive definite matrices are constrained to have positive eigenvalues, not all values in \mathbb{R}^6 can be used to generate their 6 independent components. The allowable sets of components form a curved connected submanifold of \mathbb{R}^6 . The green curve **(b)** indicates the geodesic distance between tensors in this manifold, and the olive colored dotted line shows the Euclidean distance between tensors. The dotted line is not a correct measure of the distance between tensors as it does not lie in the manifold. The bottom panel **(b)** illustrates tensors in the Log-Euclidean framework, where the symmetric positive definite matrices of the DT form a vector space. Different groups of tensors (here represented in different colors) may then be statistically compared using multivariate tests or with univariate tests on geodesic distance measures [11], [6].

6. REFERENCES

- [1] D. C. Alexander, C. Pierpaoli, P. J. Basser, and J. C. Gee, "Spatial transformations of diffusion tensor magnetic resonance," *IEEE-TMI*, 20:1131-1139, 2001.
- [2] V. Arsigny, P. Fillard, X. Pennec, and N. Ayache, "Fast and simple calculus on tensors in the log-Euclidean framework,"

in *Int Conf Med Image Comput Assist Interv.* 8:115-22, *MICCAI* 2005.

- [3] P. Batchelor, M. Moakher, D. Atkinson, F. Calamante, A. Connelly, *A rigorous framework for diffusion tensor calculus*, *Magn Reson Med.*, 53:221–225, 2005.
- [4] G. Christensen, R. Rabbitt, M. Miller. "Deformable templates using large deformation kinematics". *IEEE Trans. Image Process.* 5 1435–1447, 1996.
- [5] D. S. Falconer. *Introduction to Quantitative Genetics*. Longman, 2nd ed., 1981.
- [6] M. Jenkinson and S. Smith, "A global optimisation method for robust affine registration of brain images," *Med Image Anal*, vol. 5, pp. 143-56, 2001.
- [7] D. K. Jones, M. A. Horsfield, A. Simmons, "Optimal strategies for measuring diffusion in anisotropic systems by magnetic resonance imaging," *Magn Reson Med*, 42: 515-25, 1999.
- [8] N. Lepore, C. Brun, M.C. Chiang, Y. Chou, R.A. Dutton, K.M. Hayashi, O.L. Lopez, H. J. Aizenstein, A.W. Toga, J.T. Becker, P. Thompson, 2006. "Multivariate statistics of Jacobian matrices in Tensor Based Morphometry and their application to HIV/AIDS," *MICCAI*, 2006.
- [9] A. Pfefferbaum, E. V. Sullivan, and D. Carmelli, "Genetic regulation of regional microstructure of the corpus callosum in late life," *Neuroreport*, 12: 1677-81, 2001.
- [10] D.W. Shattuck, R.M. Leahy. *BrainSuite: an automated cortical surface identification tool*, *Medical Image Analysis* 8, (202) 129–141, 2001.
- [11] P. M. Thompson, T. D. Cannon, K. L. Narr, T. van Erp, V. P. Poutanen, M. Huttunen, J. Lonnqvist, C. G. Standertskjold-Nordenstam, J. Kaprio, M. Khaledy, R. Dail, C. I. Zoumalan, and A. W. Toga, "Genetic influences on brain structure," *Nat Neurosci*, vol. 4, pp. 1253-8, 2001.
- [12] H. Zhang, P.A. Yushkevich, D.C. Alexander, J.C. Gee, Deformable registration of diffusion tensor MR images with explicit orientation optimization. *Medical Image Analysis*. 10, 764-785, 2006.

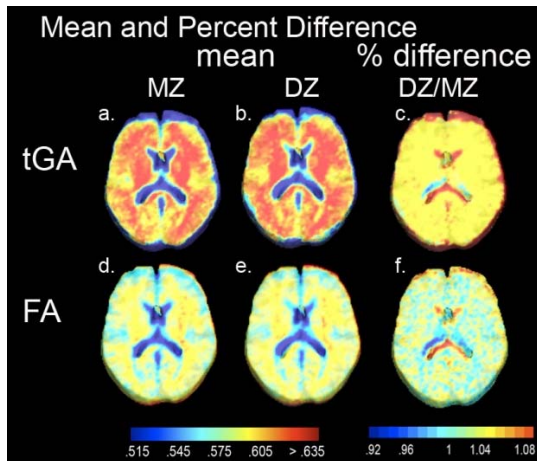


Figure 2(a) shows mean tGA images for all 44 MZ twins and **(b)** for all 46 DZ twins. **(d)** and **(e)** show mean FA image for twins of each zygosity. **(c)** and **(f)** show the ratio of the mean values for each measure, between DZ and MZ groups. Mean values for each zygosity are within a few percent of each other, as is required in a twin study (which relies on correlations *within* each group; **Fig. 3,4**).

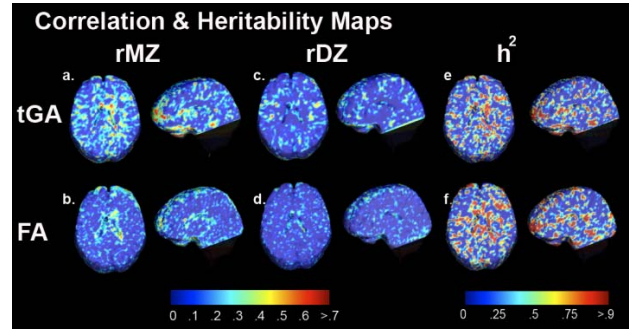


Figure 3(a)–(d): Intra-class correlation (ICC) maps for tGA and FA in MZ and DZ twins. ICC maps for MZ **(a,b)** suggest numerically greater intra-pair similarity than DZ pairs **(c,d)**. ICC maps derived from tGA **(1 and c)** have marginally greater effect sizes than those from FA **(b and d)**; see **Fig. 5**). **(e,f)** show heritability maps from tGA and from FA.

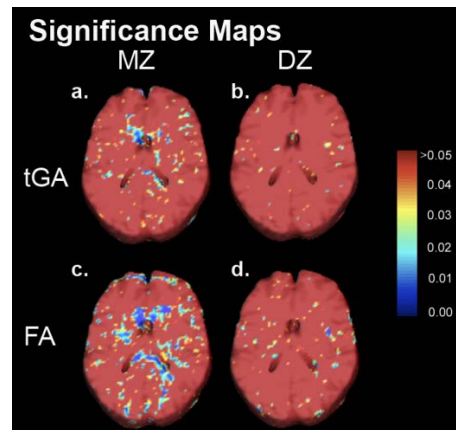


Figure 4 shows non-parametric permutation based *p*-values at each voxel, based on *r* values for tGA and FA for MZ and DZ groups. Maps based on tGA **(a, b)** and FA **(c, d)** show comparable detection power; all maps are somewhat noisy.

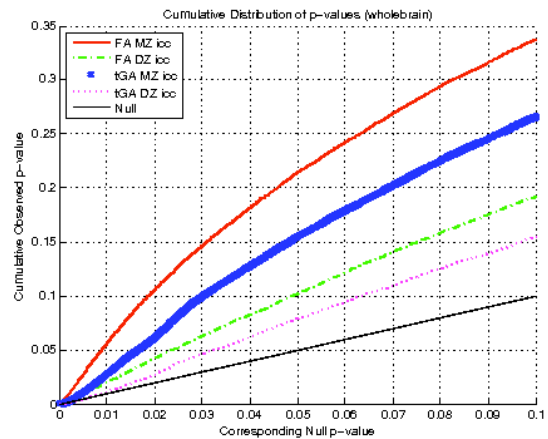


Figure 5. Cumulative distribution plots of *p*-values. Each graph shows a CDF plot for the significance of correlations, for FA and tGA, and for MZ and DZ groups. Compared with the null distribution (*solid diagonal line*), FA and GA show similar effect sizes, even though GA accounts for the tensor manifold structure in computing differences and similarities between tensors. As expected from the proportion of shared genes, effect sizes for similarities are marginally greater in identical than fraternal twins.